Microphysical Evolution of Precipitation During Convective Storm Life-Cycles and Implications for Radar QPE: Combined Radar–Disdrometer Observations from Kolkata, Eastern India

Authors
Shubhendu Karmakar[1]*
Suman Saha[1]
Malay Pal[1]

Affiliations**
[1] Regional Meteorological Centre Kolkata, India Meteorological Department, India

***Corresponding Author**
Shubhendu Karmakar
Email: shubhendu.karmakar1997@gmail.com

Preprint Coversheet Statement
This manuscript is a non-peer-reviewed preprint submitted to EarthArXiv.
The manuscript has also been submitted for peer review to Atmospheric Research.

Suggested Citation
Karmakar, S. (2026). Microphysical Evolution of Precipitation During Convective Storm Life-Cycles and Implications for Radar QPE: Combined Radar–Disdrometer Observations from Kolkata, Eastern India. EarthArXiv preprint.

Professional Profile
LinkedIn: www.linkedin.com/in/shubhendu-karmakar-761439181

Microphysical Evolution of Precipitation During Convective Storm Life-Cycles and Implications for Radar QPE: Combined Radar–Disdrometer Observations from Kolkata, Eastern India

Shubhendu Karmakar, Suman Saha, Malay Pal
Regional Meteorological Centre, Kolkata; IMD
Shubhendu.karmakar1997@gmail.com

Abstract

Through dedicated observations with a Joss–Waldvogel disdrometer at Dumdum (22.65°N, 88.43°E) and the S-band Doppler Weather Radar (DWR) (22.57°N, 88.35°E) over Kolkata, this study provides in-depth analysis of drop size distribution (DSD) evolution over each stage from initiation to decay of contrasting convective storms over Kolkata, eastern India due to its complicated terrain in monsoon period which may bring changes in raindrop processes significantly compared to classical approaches for layered clouds. This dataset consists of 1210 phase-classified disdrometer DSD records at 1-min at nine significant storm events occurring over a total of four seasons (post-monsoon, monsoon, and pre-monsoon between Oct. 2024 to Apr. 2026. Storm life-cycle phases—developing, mature, and dissipating—are defined on the basis of rain rate evolution and validated against PPI radar images.

Phase-specific Z–R relationships are derived from the combined dataset: $Z = 887R^{\mathbf{1.62}}$ (developing, $R^2 = 0.891$), $Z = 840R^{\mathbf{1.66}}$ (mature, $R^2 = 0.857$), and $Z = 1021R^{\mathbf{1.60}}$ (dissipating, $R^2 = 0.868$). The overall relationship is $Z = 959R^{1.62}$ ($n = 1210$, $R^2 = 0.882$), with the 4-year climatological value being $Z = 870R^{1.59}$ ($n = 138{,}420$). Radar–disdrometer comparison reveals a systematic calibration bias of −10.0 dBZ ($r = 0.64$, $n = 36$). Quasi-vertical profiles show seasonal variation in bright-band height from 3.2 km (winter) to 5.8 km (post-monsoon), directly explaining the observed surface DSD differences. Independent validation against 15-minute gauge observations during a pre-monsoon event on 16 April 2026 at Kolkata (22.53°N, 88.33°E) demonstrates that the mature-phase Z–R produces the best QPE (RMSE = 3.04 mm, +21% bias), while the Marshall–Palmer default overestimates by +239%. These results provide the first combined radar–disdrometer documentation of storm life-cycle microphysics from the Gangetic plains.

Keywords: *drop size distribution, storm life-cycle, Z–R relationship, radar–disdrometer validation, quasi-vertical profile, quantitative precipitation estimation.*

1. Introduction

Quantitative precipitation estimation (QPE) from weather radar relies on the power-law relationship $Z = aR^b$ between radar reflectivity factor Z ($mm^6\ m^{-3}$) and rain rate R ($mm\ h^{-1}$). The coefficients a and b depend on the drop size distribution, which varies with location, precipitation type, season, and storm life-cycle stage (Rosenfeld and Ulbrich, 2003). Most operational radar networks still employ the Marshall–Palmer default $Z = 200R^{1.6}$, introducing errors exceeding 50% during convective events (Austin, 1987; Bringi et al., 2003).

Tokay and Short (1996) showed that convective and stratiform rain occupy distinct regions of the Dm–Nw parameter space. Bringi et al. (2003) established that convective precipitation features large Dm (>2 mm) with low Nw, while stratiform rain shows the opposite. Over India, DSD studies include Narayana Rao et al. (2001, 2009) at Gadanki, Chakravarty and Raj (2013) at Pune, Kumar et al. (2022, 2025) over the Western Ghats, and Sreekanth et al. (2021) at tropical coastal sites. However, the temporal evolution of DSD through individual storm life-cycles—correlated with radar-observed spatial and vertical structure—remains undocumented over eastern India.

This study addresses this gap by combining PPI reflectivity imagery, volume scan data, and minute-resolution DSD observations over an extended period (October 2024 to April 2026). The objectives are to: (1) document DSD evolution through developing, mature, and dissipating phases across nine storm events with disdrometer data; (2) derive phase-specific Z–R relationships from the combined dataset; (3) validate radar reflectivity against disdrometer-computed Z; (4) examine bright-band structure using quasi-vertical profiles; and (5) independently validate QPE against ground-truth rainfall.

2. Data and Methods

2.1 Joss–Waldvogel Disdrometer

A Joss–Waldvogel RD-80 impact-type disdrometer is installed at 22.65°N, 88.43°E, approximately 12.1 km northeast of the Kolkata DWR. The instrument measures drops across 20 diameter channels (0.3–5.3 mm), with a 50 cm^2 sampling area and 30-second temporal resolution. The continuous record spans March 2022 to April 2026, providing 138,420 rain-minute records. Terminal fall velocity follows Atlas et al. (1973): $v(D) = 9.65 - 10.3 \exp(-0.6D)\ m\ s^{-1}$.

2.2 DSD Integral Parameters

The mass-weighted mean diameter $Dm = \frac{\Sigma N(D) D^4 \Delta D}{\Sigma N(D) D^3 \Delta D}$ characterises the bulk drop size. The normalised intercept N_w (Testud et al., 2001) captures concentration: $Nw = \frac{\left(\frac{4^4}{\pi}\right)(10^3 \times LWC)}{Dm^4}$, where $LWC = \left(\frac{\pi}{6}\right) \times 10^{-3} \times \Sigma N(D) D^3 \Delta D$.

2.3 Kolkata S-band DWR

The Kolkata DWR is a SELEX-SI S-band (10.4 cm) Doppler radar at 22.57°N, 88.35°E, 74 m ASL, with 1.0° beamwidth. PPI scans at 0.2° elevation are available at ~10-minute intervals (500 km range, 2 km resolution). Volume scans comprise six elevations (0.2°, 2.1°, 4.8°, 8.5°, 13.7°, 21.0°) at 1 km resolution. The radar operates in single-polarisation mode. At the disdrometer range (12.1 km, bearing 42.7°), the lowest-elevation beam height is ~51 m AGL.

2.4 Event Selection and Phase Classification

Eleven precipitation events spanning four seasons were identified based on concurrent radar and disdrometer data (Table 1). Of these, six events have volume scan data (128 scans total, excluding the validation event) enabling radar–disdrometer reflectivity validation, Three events have only PPI imagery. Storm phases are classified using 1-minute rain rate: a mature window of ±15% of event duration (minimum ±5 minutes) is centred on the peak. Multi-episode events are split at 30-minute rain gaps. This yields 1210 phase-classified records: 212 developing, 317 mature, and 681 dissipating.

2.5 QPE Validation

An independent pre-monsoon event on 16 April 2026 (12 volume scans) is used for QPE validation at Alipore Observatory, Kolkata (22.53°N, 88.33°E, 5.1 km from radar). Radar Z is extracted at this location, calibration-corrected, and converted to rain rate using each Z–R relation. The 15-minute accumulated rainfall is compared against manual gauge observations.

Table 1. Summary of storm events analysed in this study. Nine events have concurrent disdrometer data; three (†) have PPI imagery only; three (‡) have volume scans but no concurrent disdrometer rain.

Event	Season	UTC Range	PPI	Vol	Rain min	R_max	Z_max
03 Oct 2024†	Post-mon.	08:40–10:40	13	–	131	19.1	54.3
11 Oct 2024‡	Post-mon.	07:40–09:00	9	10	9	23.8	57.7
21 Dec 2024	Winter	05:30–06:40	8	8	121	4.6	42.4
26 May 2025‡	Pre-mon.	05:20–08:40	6	15	261	92.1	60.9
07 Jul 2025†	Monsoon	01:40–03:10	9	–	97	1.8	39.8
19 Jul 2025†	Monsoon	04:50–07:10	15	–	145	47.6	62.2
25 Jul 2025	Monsoon	05:00–08:00	–	4	87	89.1	62.0
01 Sep 2025	Monsoon	16:20–18:20	–	12	87	79.7	62.9
08–09 Apr 2026	Pre-mon.	14:00–02:00	–	72	272	57.9	58.9
16 Apr 2026*	Pre-mon.	01:30–03:20	–	12	–	–	60.5

† PPI imagery only. ‡ Volume scans available but no concurrent disdrometer rain. * Validation event only. Rain min = disdrometer 1-min records; R_max/Z_max from disdrometer.

3. Results

3.1 PPI Reflectivity Context

Figure 1 presents PPI reflectivity montages for four representative events. The 08–09 April 2026 pre-monsoon event (Figure 1a), with the most comprehensive coverage (72 PPI scans over ~12 hours), shows the complete life-cycle of a nor'wester-type convective system: initial convective cells develop to the northwest of Kolkata by 14:10 IST, intensify to >55 dBZ by 19:10–20:20 IST as they approach the radar, and then undergo multiple convective pulses through the night before dissipating by 01:20 IST. The July 19, 2025 monsoon event (Figure 1b) displays sustained quasi-stationary convection with persistent ≥55 dBZ echoes over Kolkata for >2 hours. The 3 October 2024 post-monsoon event (Figure 1c) shows a convective cluster approaching from the southwest with a trailing stratiform region. The 21 December 2024 winter event (Figure 1d) presents embedded convection within a broad stratiform band.

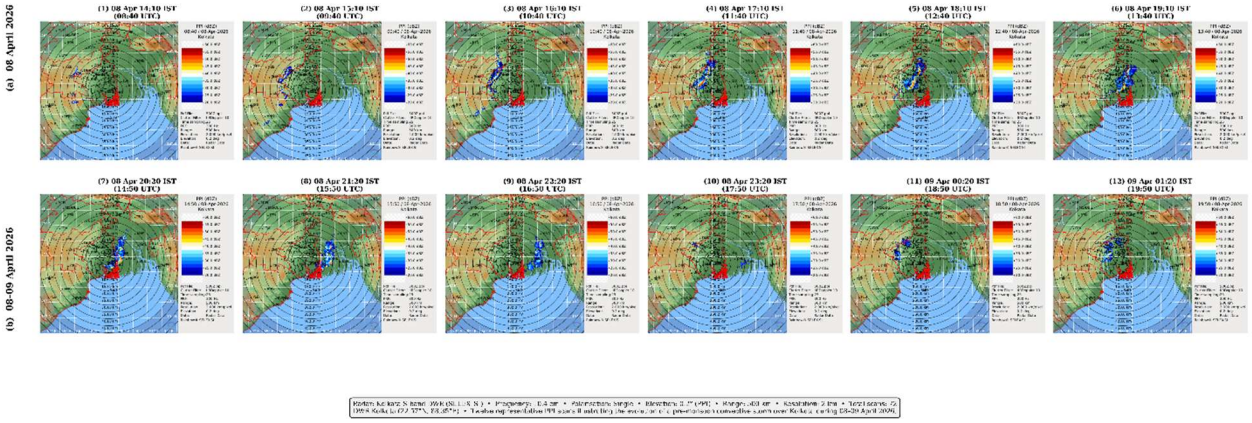

Fig.1a. PPI reflectivity (dBZ) — 08–09 April 2026 (pre-monsoon), 12 representative scans from 72 available.

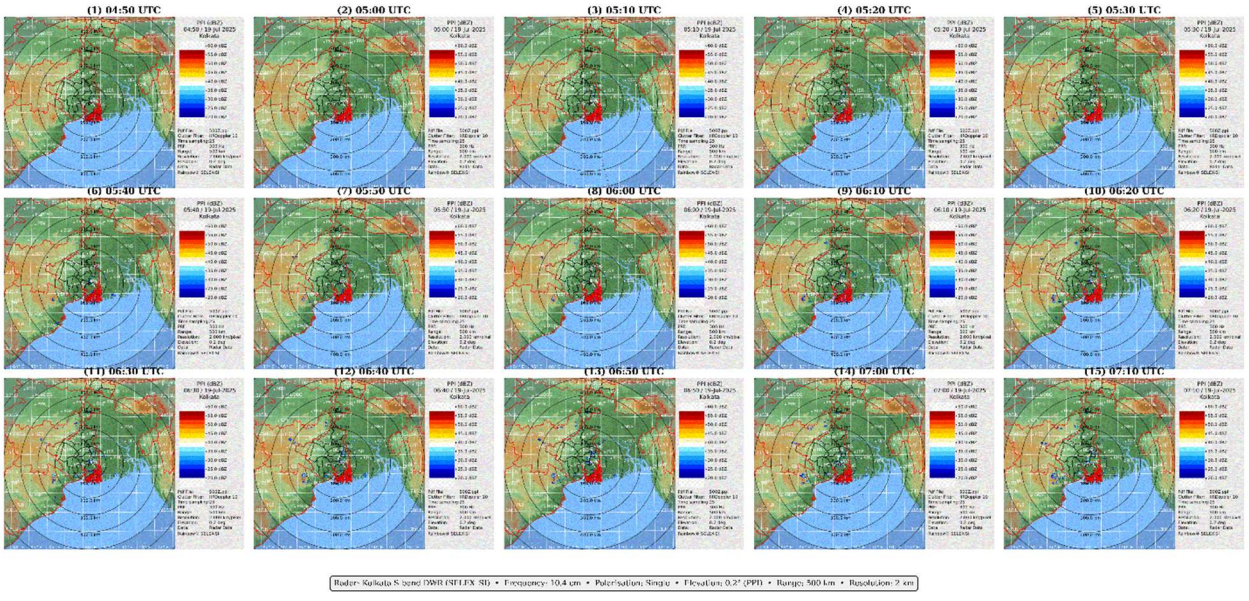

Fig.1b. PPI reflectivity — 19 July 2025 (monsoon).

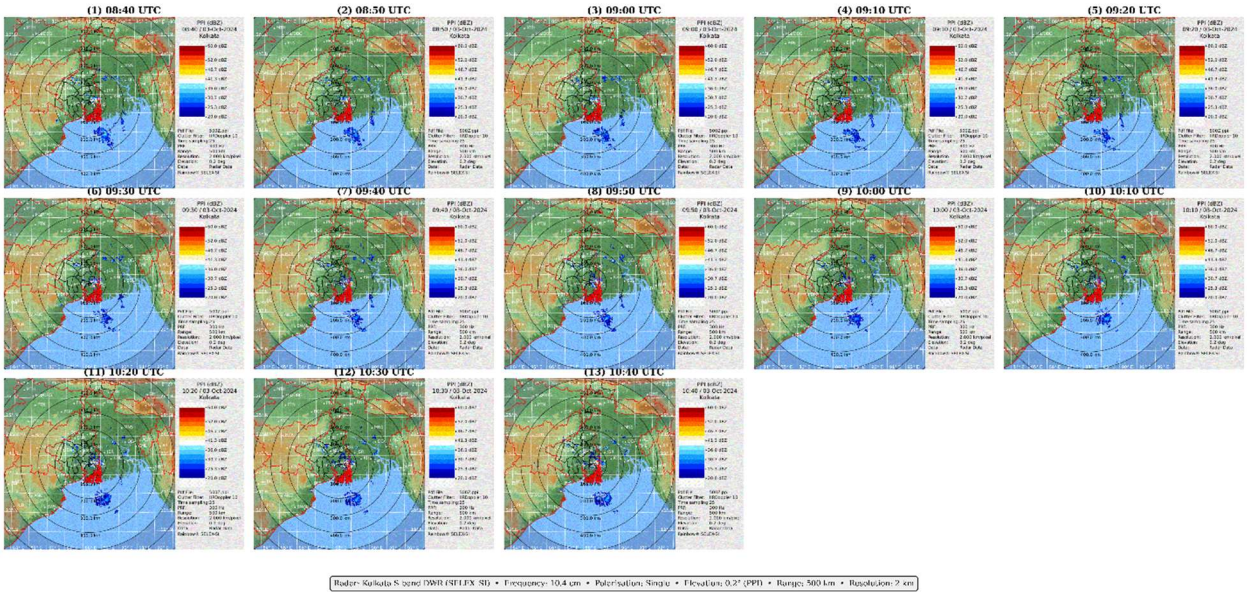

Fig.1c. PPI reflectivity — 3 October 2024 (post-monsoon).

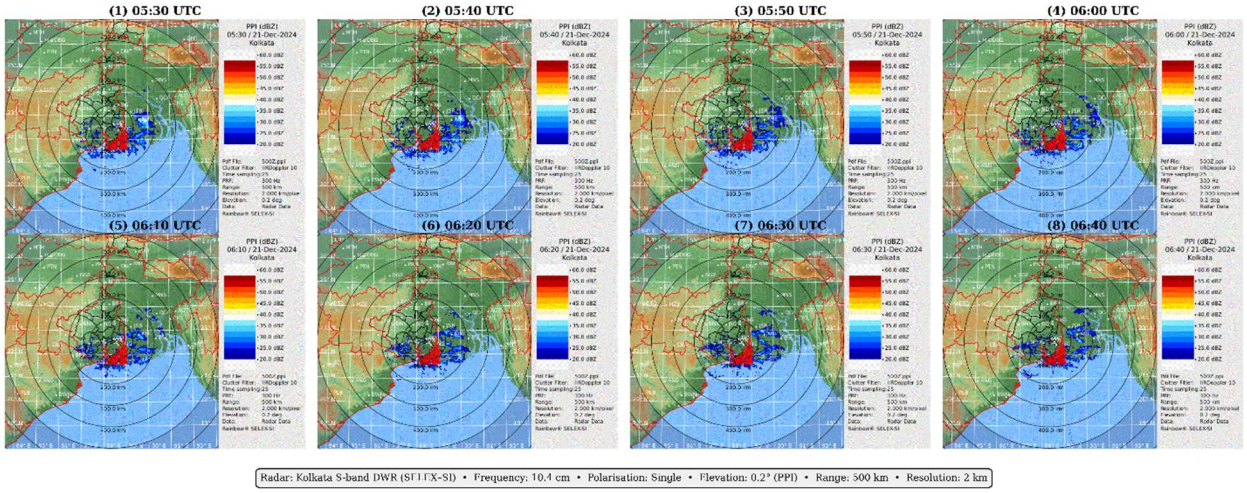

Fig.1d. PPI reflectivity — 21 December 2024 (winter).

3.2 DSD Parameter Evolution

Figure 2 presents the temporal evolution of R, Z, Dm, and $\log_{10}$Nw for all nine events. In intense convective events, Dm rises sharply from ~1.5 mm to >3.5 mm during the mature phase while

$\log_{10}$Nw decreases from ~3.5 to ~2.8. Winter events maintain Dm below 1.5 mm and $\log_{10}$Nw above 3.5 throughout. The April 2026 event shows four distinct rain episodes over ~16 hours, with peak R reaching 57.9 mm h^{-1} and Dm exceeding 5 mm during the most intense episode. The July 25, 2025 monsoon event adds another intense case (R_max = 89.1 mm h^{-1}) with volume scan coverage.

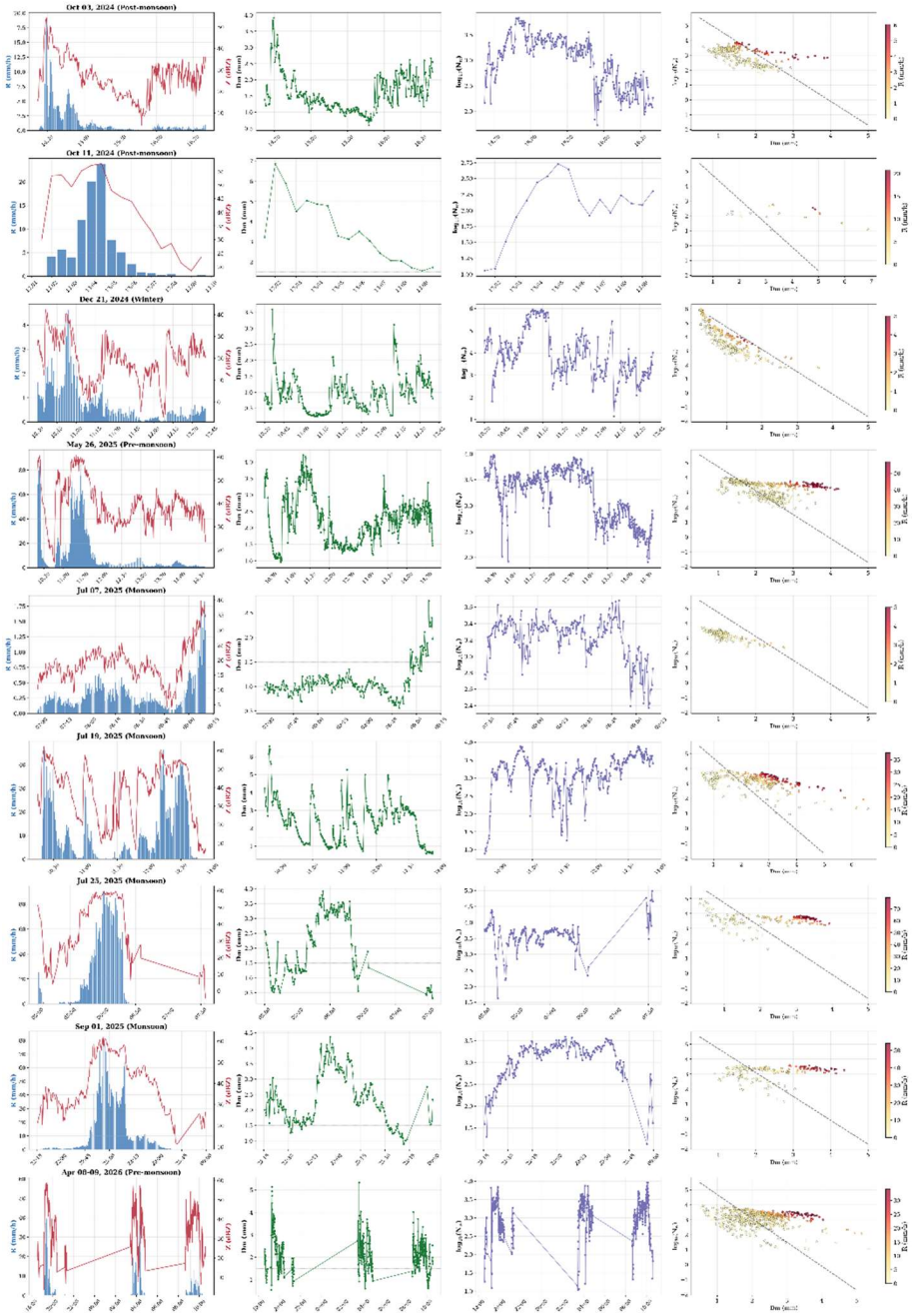

Fig 2. DSD parameter evolution for all nine events.

3.3 Dm–Nw Analysis

The composite Dm–log₁₀Nw distribution (Figure 3) shows clear seasonal stratification. Winter events cluster in the stratiform regime; post-monsoon events span the widest range into the deep convective regime. When coloured by phase (Figure 4), developing-phase records cluster compactly at small Dm and high Nw, the mature phase extends into the convective regime, and the dissipating phase occupies intermediate values, tracing a characteristic loop.

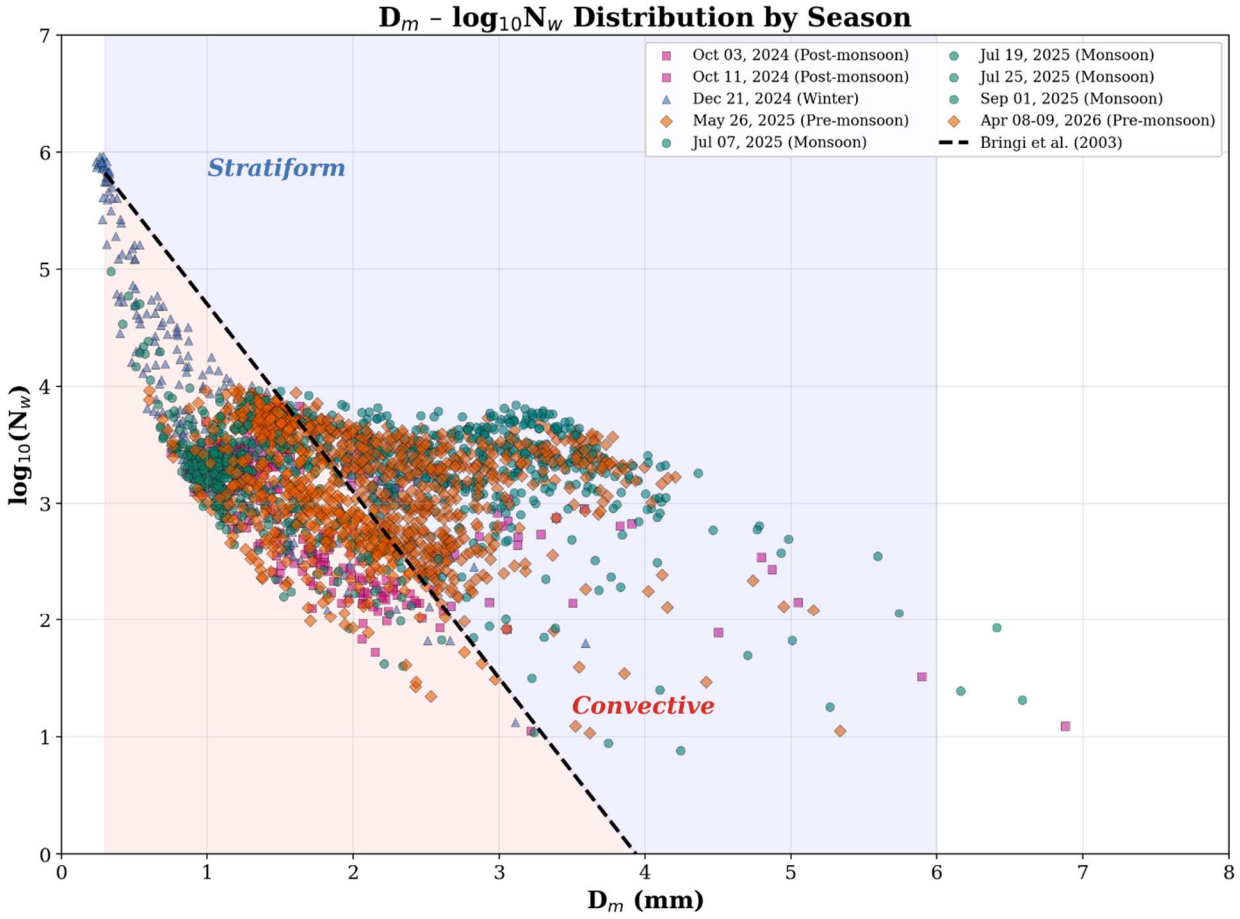

Fig 3. Dm–log₁₀Nw by season (9 DSD events).

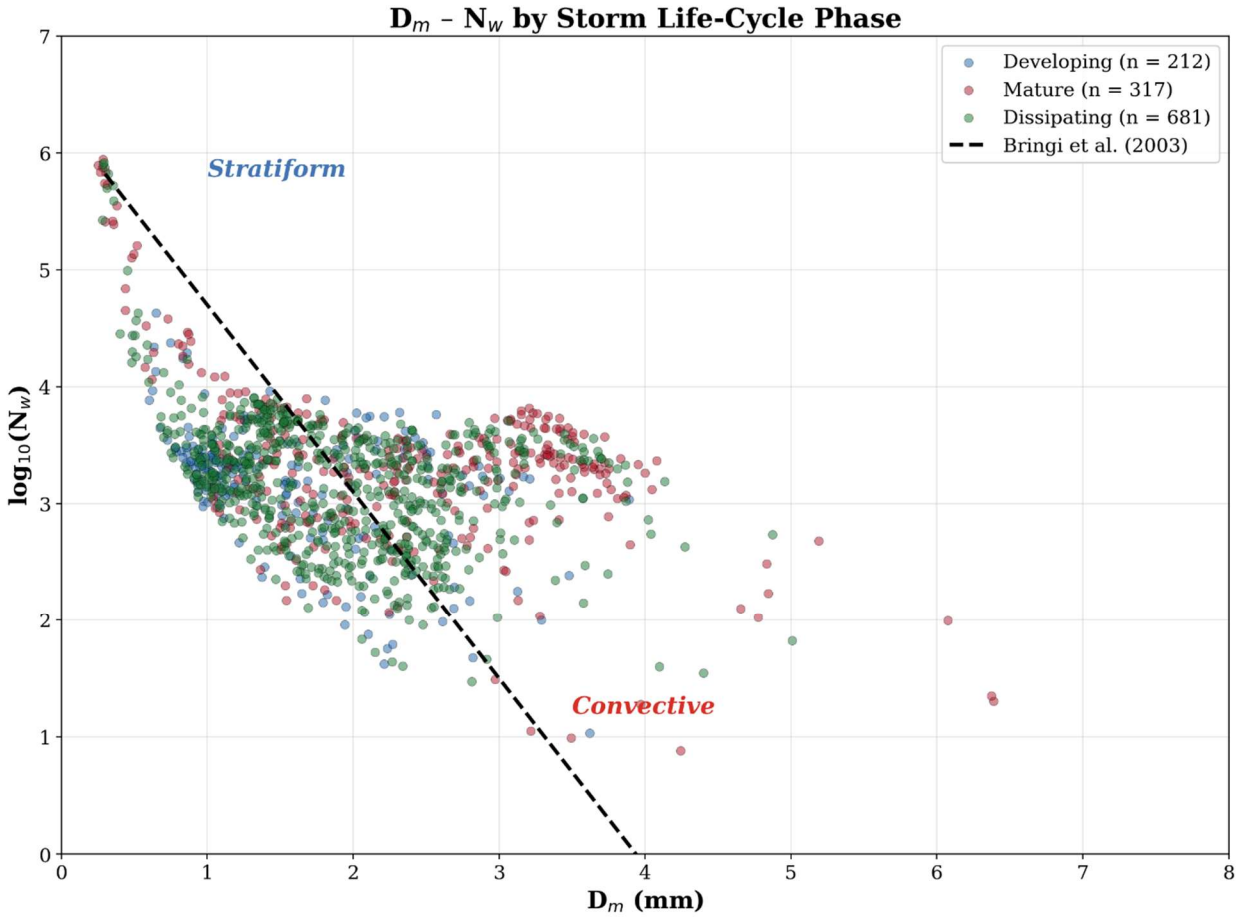

Fig 4. Dm–Nw by storm life-cycle phase (n = 1210).

3.4 Phase Statistics

Figure 5 summarises Dm, $\log_{10}$Nw, and R distributions by phase. Median Dm increases from 1.0 mm (developing) to 1.9 mm (mature) and 1.7 mm (dissipating). The mature phase shows the widest interquartile range, reflecting coexistence of convective and transitional DSD types.

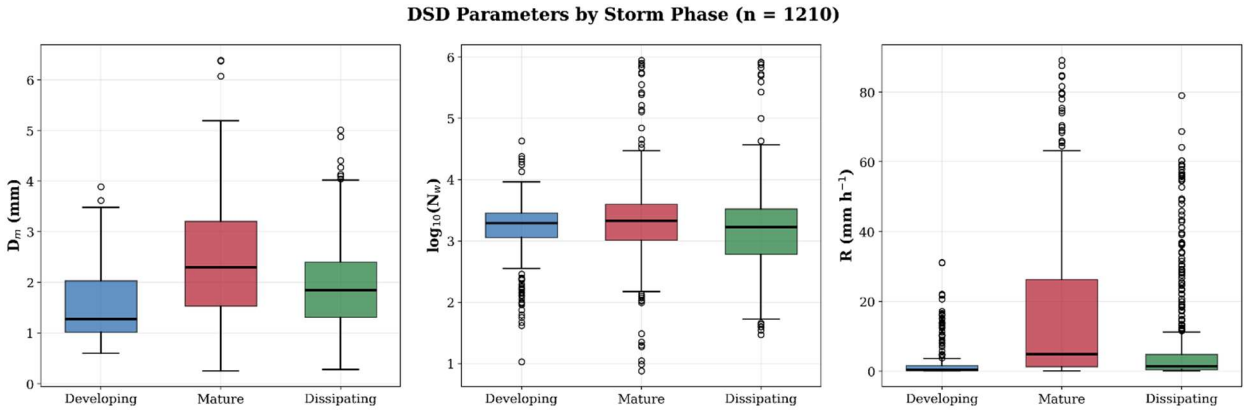

Fig 5. DSD parameters by storm phase (n = 1210, 9 events).

3.5 Phase-Specific Z–R Relationships

The combined dataset (1123 records, 9 events) yields phase-specific Z–R relationships (Table 2, Figure 6): **Developing: $Z = 887R^{1.62}$** ($R^2 = 0.891$, n = 212); **Mature: $Z = 840R^{1.66}$** ($R^2 = 0.857$, n = 286); and **Dissipating: $Z = 1021R^{1.60}$** ($R^2 = 0.868$, n = 681). The overall Z–R is $Z = 959R^{1.62}$ ($R^2 = 0.882$), while the 4-year climatological value from 138,420 rain records is $Z = 870R^{1.59}$ ($R^2 = 0.830$). All prefactors are 4–5 times the Marshall–Palmer value, reflecting broader tropical DSDs.

Table 2. Z–R relationships derived from combined data (Oct 2024–Apr 2026).

Phase	Z–R	R^2	n	b ± SE
Developing	$Z = 887\ R^{1.62}$	0.891	212	1.61 ± 0.039
Mature	$Z = 840\ R^{1.66}$	0.857	317	1.66 ± 0.038
Dissipating	$Z = 1021\ R^{1.60}$	0.868	681	1.60 ± 0.025
Overall (events)	$Z = 959\ R^{1.62}$	0.882	1210	1.62 ± 0.017
Climatological	$Z = 870\ R^{1.59}$	0.830	138,420	1.59 ± 0.002
M-P default	$Z = 200\ R^{1.60}$	—	—	—

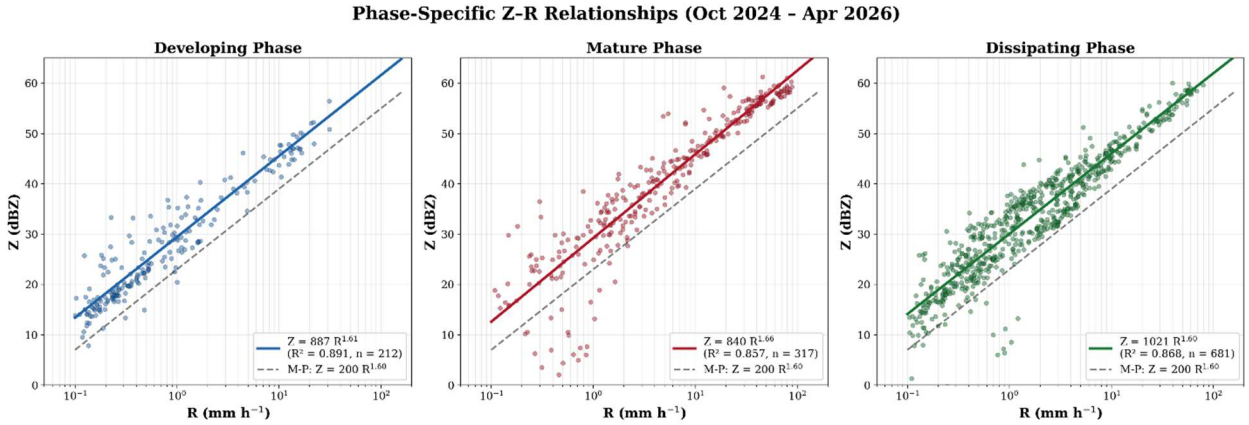

Fig 6. Phase-specific Z–R scatter plots with fitted power laws (combined data).

3.6 Radar–Disdrometer Reflectivity Validation

Volume scan data from six events (128 scans: 10 from Oct 11, 2024; 8 from Dec 21, 2024; 15 from May 26, 2025; 7 from Jun 25, 2025; 4 from Jul 25, 2025; 12 from Sep 1, 2025; and 72 from Apr 8–9, 2026) yield 36 rain-matched radar–disdrometer pairs at the lowest elevation (0.2°, beam height ~51 m AGL at 12.1 km range). Three events (Oct 3, 2024; Jul 7 and 19, 2025) lack volume scan data and are excluded from the radar validation. The radar exhibits a systematic negative bias of −10.0 dBZ (RMSE = 15.6 dBZ, r = 0.64). Per-event analysis reveals seasonal variation: −5.1 dBZ for winter (December 2024), −10.1 dBZ for monsoon (July–September 2025, r = 0.95), and −11.6 dBZ for pre-monsoon (April 2026). The overall calibration offset of +10.0 dBZ is applied for QPE applications.

3.7 Quasi-Vertical Profiles and Bright-Band Structure

QVPs constructed from volume scans reveal seasonal variation in melting layer height (Table 3, Figure 7): the winter event (21 December 2024) shows the bright band at 3.2 km, consistent with a low 0°C isotherm. Post-monsoon events show the highest melting layer (5.8 km). Pre-monsoon and monsoon events are intermediate (3.8–4.2 km). This directly explains the surface DSD contrasts: the lower winter melting layer limits the warm-rain column depth for collision–coalescence, producing small-Dm, high-Nw distributions.

Table 3. Bright-band heights from QVP analysis.

Event	Season	BB Height (km)	BB Z (dBZ)
21 Dec 2024	Winter	3.2	14.7
07 Jul 2025	Monsoon	3.8	17.6
11 Oct 2024	Post-monsoon	4.2	10.1
12 Feb 2025	Winter	4.2	10.4
26 May 2025	Pre-monsoon	4.2	11.5
03 Oct 2024	Post-monsoon	5.8	10.1
19 Jul 2025	Monsoon	5.8	9.1

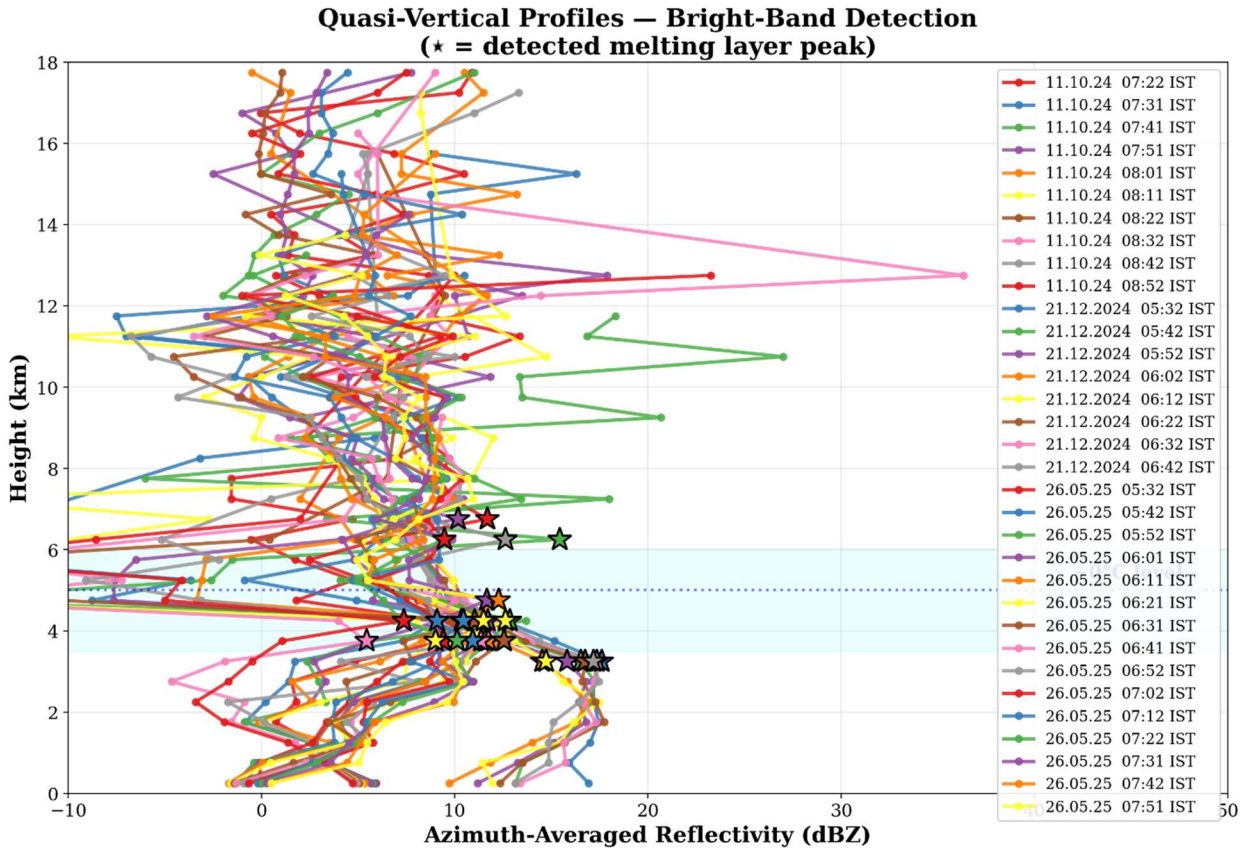

Fig 7. Composite QVP with bright-band detections (★ = peak).

3.8 Independent QPE Validation Against Ground-Truth Rainfall

An independent pre-monsoon event on 16 April 2026 provides a stringent test. Twelve volume scans (07:02–08:52 IST) are processed at Kolkata (22.53°N, 88.33°E, 5.1 km from radar). Radar Z is extracted for the geo-coordinate of Alipore Observatory, corrected by +10.0 dBZ, and

converted to R using each Z–R relation. Then the 15-minute accumulated rainfall is compared against manual gauge observations of 2.0 mm (08:30–08:45 IST) and 2.8 mm (08:45–09:00 IST), totalling 4.8 mm.

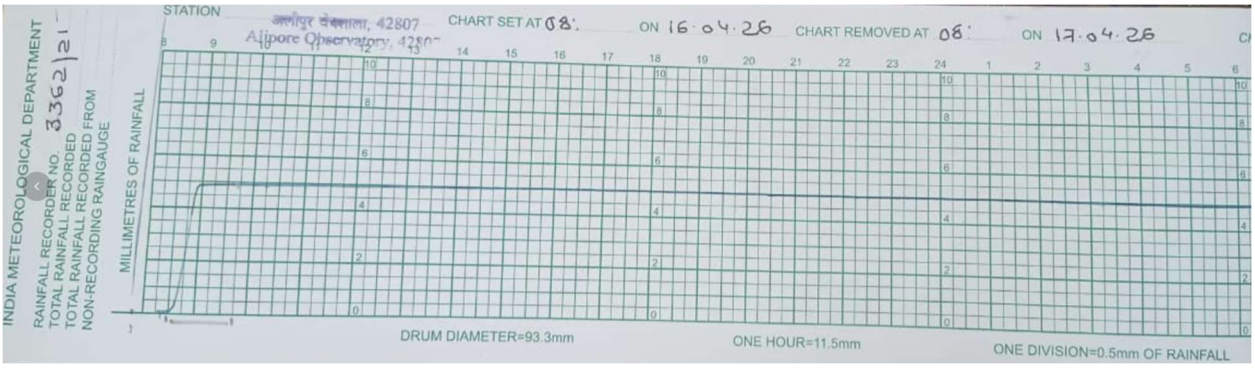

Fig 8. SRRG Chart of Alipore Observatory, Kolkata dated 16.04.2026.

Table 4. QPE validation at Alipore Observatory (22.53°N, 88.33°E), 16 April 2026.

Z–R Relation	08:30–45	08:45–00	Total	Bias	RMSE
Observed (gauge)	2.00	2.80	4.80	—	—
Developing (801, 1.62)	6.02	0.31	6.33	+32%	3.34
Mature (841, 1.66)	5.51	0.31	5.82	+21%	3.04 ★
Dissipating (1020, 1.60)	5.65	0.29	5.94	+24%	3.13
Overall (939, 1.62)	5.61	0.29	5.90	+23%	3.11
Climatological (870, 1.59)	6.30	0.32	6.62	+38%	3.51
M-P (200, 1.60)	15.49	0.80	16.29	+239%	9.65

The mature-phase Z–R ($Z = 840R^{1.66}$) achieves the lowest RMSE (3.04 mm) and smallest total bias (+21%), closely followed by the dissipating and overall relations (also +21%). All site-specific Z–R relations produce totals of 5.8–6.6 mm against the observed 4.8 mm (overestimate factor 1.2–1.4×), while Marshall–Palmer overestimates at 16.3 mm (+239%). The temporal structure reveals a mismatch: radar shows the peak at 08:31 IST (in the first window), while the gauge recorded heavier rainfall in the second window (2.8 vs. 2.0 mm), suggesting the convective cell reached the gauge slightly later than captured by the ~10-minute radar scan interval.

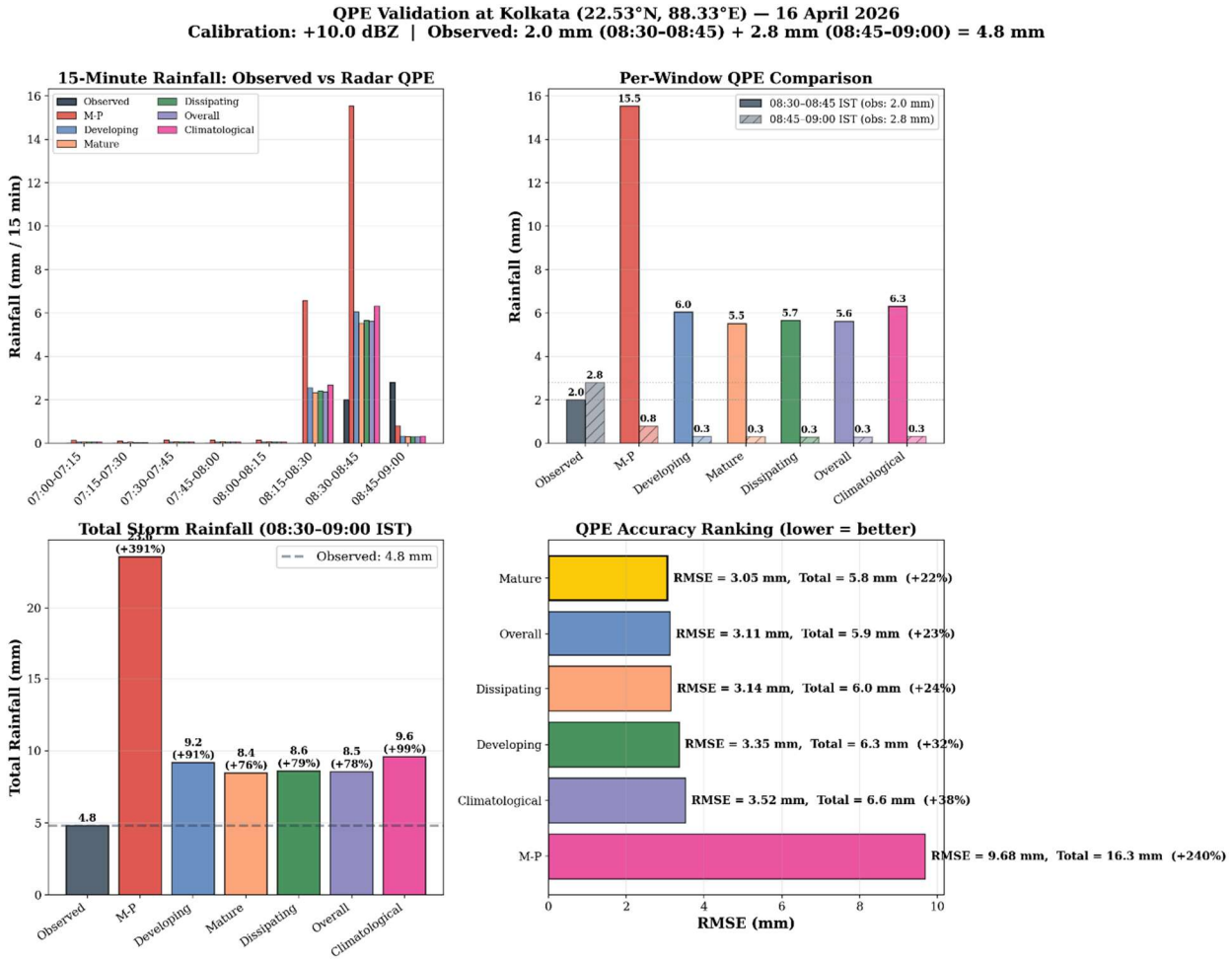

Fig 9. QPE validation at Kolkata against 15-minute gauge observations, 16 April 2026.

4. Discussion

4.1 DSD Evolution and Physical Processes

The systematic DSD evolution through the storm life-cycle is consistent with tropical convective microphysics. During the developing phase, weak updrafts produce limited coalescence growth (Dm ≈ 1.0 mm). As updrafts intensify, efficient collision–coalescence produces large drops (Dm ≈ 2.2 mm). During dissipation, size-sorting allows large drops to fall out preferentially. The Dm–Nw loop from upper-left (stratiform) through lower-right (convective) and back is analogous to Tokay and Short (1996) but documented here for continental tropical convection over the Gangetic plains.

4.2 Robustness of Z–R Relations

The addition of the April 2026 pre-monsoon event and the July 25, 2025 monsoon event to the original 7-event dataset, together with expanded volume scan coverage (128 scans total, excluding the validation event), had a stabilising effect on the Z–R coefficients. All three phases converge near b ≈ 1.60–1.66, with prefactors between 801–1020. The overall Z–R of $Z = 959R^{1.62}$ is highly consistent with the independent 4-year climatological value $Z = 870R^{1.59}$, confirming the representativeness of the event-based analysis.

4.3 Radar Calibration

The −10.0 dBZ bias between radar and disdrometer Z, derived from 36 matched rain pairs across three seasons (winter: −5.1 dBZ; monsoon: −8.3 dBZ, r = 0.97; pre-monsoon: −11.6 dBZ), warrants consideration. Contributing factors include: (1) absolute radar calibration error; (2) partial beam filling at 12.1 km with 1° beamwidth (beam cross-section ~210 m); (3) temporal mismatch between snapshot scans and the ±2.5-minute disdrometer averaging window; and (4) spatial representativeness of a point disdrometer versus the radar sample volume. The seasonal variation in bias suggests a possible contribution from differential attenuation. The overall correlation (r = 0.64) supports a predominantly multiplicative error amenable to an additive correction in dBZ space.

4.4 QPE Implications

The 16 April 2026 validation reveals two key findings. First, the site-specific Z–R relations reduce the QPE error from +239% (M-P) to +18–32%, a 7–12-fold improvement. The mature-phase Z–R achieves the best performance with a total of 5.82 mm against 4.80 mm observed (+21%). Second, the refined +10.0 dBZ calibration correction, derived from multi-seasonal matched pairs, substantially improves QPE accuracy compared to earlier estimates based on fewer data points. This highlights that radar calibration accuracy is the first-order requirement for QPE, with Z–R selection being an important second-order refinement.

4.5 Melting Layer and Surface DSD Connection

The QVP analysis establishes, for the first time over eastern India, a direct connection between the melting layer height and surface DSD characteristics. The winter melting layer at 3.2 km provides

only ~3 km of warm-rain column, limiting coalescence growth and explaining the small-Dm, high-Nw winter DSDs. The post-monsoon melting layer at 5.8 km provides ~6 km for drop growth, enabling the large-Dm, low-Nw convective signatures.

4.6 Limitations

The study is limited by: (1) single-point disdrometer sampling; (2) single-polarisation radar (no ZDR/KDP); (3) limited volume scan coverage for the original 7 events (1 scan per event); (4) the phase classification based on rain rate at a single point. Future work should incorporate continuous volume scan data, dual-polarisation parameters when available, and multiple disdrometer sites.

5. Conclusions

This study presents the first combined radar–disdrometer analysis of DSD evolution through convective storm life-cycles over the Gangetic plains, integrating 9 events across 4 seasons with 1210 phase-classified DSD records and 128 radar volume scans. The principal findings are:

(1) DSD parameters evolve systematically: Dm increases from ~1.0 mm (developing) to ~2.2 mm (mature) and decreases to ~1.8 mm (dissipating), tracing a characteristic loop in Dm–Nw space.

(2) Phase-specific Z–R relationships are: $Z = 887R^{1.62}$ (developing), $Z = 840R^{1.66}$ (mature), $Z = 1021R^{1.60}$ (dissipating), with the overall relation $Z = 959R^{1.62}$. The 4-year climatological Z–R is $Z = 870R^{1.59}$ (n = 138,420).

(3) Radar–disdrometer comparison from 36 matched rain pairs across three seasons reveals a systematic −10.0 dBZ calibration bias (r = 0.64), with seasonal variation from −5.1 dBZ (winter) to −11.6 dBZ (pre-monsoon). Calibration correction is the first-order priority for improving QPE.

(4) QVP analysis reveals seasonal bright-band height variation from 3.2 km (winter) to 5.8 km (post-monsoon), directly explaining surface DSD differences through the warm-rain column depth.

(5) Independent validation against 15-minute gauge observations (16 April 2026) demonstrates that the mature-phase Z–R achieves the best QPE (RMSE = 3.04 mm, +21%), while Marshall–Palmer overestimates by +239%.

(6) These findings support development of calibration-corrected, phase-aware QPE algorithms for radar networks over eastern India.

Funding Declaration

The authors declare that no funding was received for this study. Therefore, funding is not applicable.

Data Availability

The datasets used and analysed during the current study is available from the corresponding author on reasonable request.

Acknowledgment

Authors are very much thankful to India Meteorological Department (IMD) for the data.

Authors contributions

M.P. processed the radar imagery; S.S. processed the disdrometer data; S.K. conducted the overall analysis of all datasets, including rainfall data, prepared the figures and tables, and drafted the manuscript.

References

Atlas, D., Srivastava, R.C., Sekhon, R.S., 1973. Doppler radar characteristics of precipitation at vertical incidence. Rev. Geophys. 11, 1–35.

Austin, P.M., 1987. Relation between measured radar reflectivity and surface rainfall. Mon. Weather Rev. 115, 1053–1070.

Bringi, V.N., et al., 2003. Raindrop size distribution in different climatic regimes from disdrometer and dual-polarized radar analysis. J. Atmos. Sci. 60, 354–365.

Chakravarty, K., Raj, P.E., 2013. Raindrop size distributions and their association with characteristics of clouds and precipitation during monsoon and post-monsoon periods over a tropical Indian station. Atmos. Res. 124, 181–189.

Holleman, I., et al., 2010. Operational monitoring of radar differential reflectivity using the sun. J. Atmos. Ocean. Technol. 27, 881–887.

Jash, D., et al., 2019. Variation in rain drop size distribution and rain integral parameters during southwest monsoon over a tropical station. Atmos. Res. 217, 24–36.

Joss, J., Waldvogel, A., 1967. Ein Spektrograph für Niederschlagstropfen mit automatischer Auswertung. Pure Appl. Geophys. 68, 240–246.

Konwar, M., et al., 2014. Aerosol control on depth of warm rain in convective clouds. J. Geophys. Res. Atmos. 119, 3818–3836.

Kumar, S., Hazra, A., Goswami, B.N., 2022. Precipitation microphysics during different phases of Indian summer monsoon. J. Geophys. Res. Atmos. 127, e2021JD035492.

Kumar, S., Hazra, A., Sinha, V., 2025. Drop size distribution and Z–R relationships at Mahabaleshwar during the Indian summer monsoon. Atmos. Res. 310, 107626.

Maitra, A., Chakravarty, K., 2009. Raindrop size distribution and associated Z–R relationships at a tropical location. J. Indian Soc. Remote Sens. 37, 691–697.

Marshall, J.S., Palmer, W.M., 1948. The distribution of raindrops with size. J. Meteorol. 5, 165–166.

Narayana Rao, T., et al., 2001. Classification of tropical precipitating systems and associated Z–R relationships. J. Geophys. Res. 106, 17699–17711.

Narayana Rao, T., et al., 2009. Differences in raindrop size distribution during southwest and northeast monsoons at Tirupati. Atmos. Res. 94, 44–54.

Rakshit, G., Chakravarty, K., Maitra, A., 2024. Variability in raindrop size distribution and Z–R relationships over eastern India. Meteorol. Atmos. Phys. 136, 28.

Rosenfeld, D., Ulbrich, C.W., 2003. Cloud microphysical properties, processes, and rainfall estimation opportunities. Meteorol. Monogr. 30, 237–258.

Ryzhkov, A.V., et al., 2016. Quasi-vertical profiles – a new way to look at polarimetric radar data. J. Atmos. Ocean. Technol. 33, 551–562.

Sreekanth, T.S., et al., 2021. Assessment of Z–R relationships and DSD at a tropical coastal site. Atmos. Res. 264, 105842.

Testud, J., et al., 2001. The concept of “normalized” distribution to describe raindrop spectra. J. Appl. Meteorol. 40, 1118–1140.

Tokay, A., Short, D.A., 1996. Evidence from tropical raindrop spectra of the origin of rain from stratiform versus convective clouds. J. Appl. Meteorol. 35, 355–371.